X-ray emission cross sections following charge exchange by multiply charged ions of astrophysical interest

S. Otranto,[1,*] R. E. Olson,[1] and P. Beiersdorfer[2]
[1]*Physics Department, University of Missouri-Rolla, Rolla Missouri 65401, USA*
[2]*Department of Physics, Lawrence Livermore National Laboratory, Livermore, California 94550, USA*
(Received 2 September 2005; revised manuscript received 30 November 2005; published 27 February 2006)

State selective *nl*-electron capture cross sections are presented for highly charged ions with $Z=6-10$ colliding with atoms and molecules. The energy range investigated was from 1 eV/amu($v=0.006$ a.u.) to 100 keV/amu($v=2.0$ a.u.). The energy dependence of the *l*-level populations is investigated. The *K* shell x-ray emission cross sections are determined by using the calculated state-selective electron capture results as input and then applying hydrogenic branching and cascading values for the photon emission. A major shift in the line emission from being almost solely Lyman-α transitions at the highest collisions energies to strong high-*n* to 1*s* transitions at the lowest energies is observed. The calculated cross sections are in reasonable accord with measurements made by Greenwood *et al.* [Phys. Rev. A **63**, 062707 (2001)], using O^{8+} and Ne^{10+} on various targets at 3 keV/amu. The calculations are also in accord with x-ray emission cross section data obtained on the EBIT machine at Lawrence Livermore National Laboratory (LLNL) where O^{8+} and Ne^{10+} high resolution measurements were made at a temperature of 10 eV/amu for a series of targets with varying ionization potentials. The Ne^{10+} data clearly shows the contribution from multiple capture followed by Auger autoionization in the line emission spectra. Our calculated line emission cross sections are used to provide an *ab initio* determination of the soft x-ray spectrum of comet C/Linear 1999 S4 that was observed on the Chandra X-ray Observatory. The calculations show that the spectrum is due to the charge exchange of the neutral gases in the comet's coma with the ions of the slow solar wind.

DOI: 10.1103/PhysRevA.73.022723 PACS number(s): 34.70.+e, 32.30.Rj, 32.70.Fw, 95.30.Ky

I. INTRODUCTION

State-selective single electron capture induced by highly stripped multiply charged ions colliding with atoms and molecules in general produces an excited ion that decays via photon emission,

$$A^{q+} + B \rightarrow A^{(q-1)+*}(nl) + B^{+}, \tag{1}$$

$$A^{(q-1)+*}(nl) \rightarrow A^{(q-1)+} + h\nu. \tag{2}$$

For low to intermediate collision energies, $E<25$ keV/amu, several theoretical methods can be used to estimate the capture cross sections. Quantum mechanical techniques such as the atomic and molecular orbital methods provide accurate values for systems, where the basis sets can be of reasonable size, such as for charge states $q<8$ and atomic H and He targets at energies where the ionization continuum is unimportant [1,2]. Simpler methods such as the multichannel Landau-Zener (LZ) [3], and classical trajectory Monte Carlo (CTMC) methods [4,5] allow greater flexibility in the choice of reactants, yet provide general scaling relationships that are valuable when theoretical input is required for complex systems such as molecular targets or high charge state projectiles [6].

The LZ and CTMC methods early on predicted the total cross section for the reaction Eq. (1) with hydrogen targets scaled linearly in charge state and was independent of energy for high charge state projectiles, with a magnitude of roughly $\sigma \sim q \times 10^{-15}$ cm^2 [3,7,8]. CTMC calculations showed that the most probable principal quantum number for capture was

$$n_p = n_i q^{3/4}, \tag{3}$$

where n_i is the initial level of a hydrogen target and q the charge state of the projectile [9]. Equation (3) can be generalized to other targets by using hydrogenic scaling of the ionization potentials (IP) to yield

$$n_p = \left(\frac{13.6 \text{ eV}}{V_{\text{ion}}}\right)^{1/2} q^{3/4}. \tag{4}$$

However, even though the total and *n*-selective cross sections can be qualitatively predicted, the *l* orbital angular momentum levels produced by electron capture are more elusive. They not only depend on where in the *n* manifold they are associated, but are also a function of the collision energy [9]. In general, the *l* levels tend to be populated statistically, $2l+1$, at the higher energies, while low values of *l* dominate for very slow collisions. For line emission cross sections Eq. (2), the energy dependence of the *l* sublevels is, of course, of crucial importance.

Line emission cross sections calculated using the CTMC method for hydrogen targets have a long history. They are used as the basis for diagnostics on tokamak fusion plasmas to determine the concentrations of highly charged impurity ions [10,11]. The spectra themselves are used to estimate the plasma temperature by measuring the broadening of the specific spectral lines, along with determining the plasma rotation via the Doppler shift of the lines. However, the CTMC calculations have generally been only applied and tested at intermediate collision energies, 1–40 keV/amu, because these energies correspond to the injection energy of a toka-

mak fueling and heating H or D neutral beam. Within the CTMC method, semiclassical methods have been developed, and tested, to predict the n, l, and m_l electron capture excited levels [12]. These collision codes have been married to those that follow the dipole allowed photon transitions of the excited states during their branching and cascading to the ground level. It is this suite of codes that we utilize in this work.

Motivation for the current work is provided by recent observations of x-ray emission from comets as they transit our solar system. It is now recognized that the x-rays arise from electron capture collisions between multiply charged ions in the solar wind and the gases, (H_2O, CH_4, CO, and CO_2 among others), surrounding the comet [13]. The energy range of interest is approximately 0.8 keV/amu for the slow solar wind ions, and 3.0 keV/amu for the fast solar wind components. The solar wind ions that dominate soft x-ray emission are primarily high charge states of carbon and oxygen, with some nitrogen. To date, astrophysical models for the electron capture reactions have assumed equal population of the l-values, or statistical populations, where the ion deexcites via photon cascades along the yrast chain $\Delta n=-1$ that primarily produces just the Lyman-α transition [14–16]. Other work has been based on Landau-Zener calculations with the l-values adjusted to reproduce available data [17,18].

It is the purpose of this paper to provide general insight into the dependence of the populated orbital angular momentum levels as a function of collision energy from 1 eV/amu to 100 keV/amu. Such calculations provide the basis on what to expect for the ratio of Lyman-α to $np \rightarrow 1s$ $(n>2)$ x-ray transitions, the latter of which are important components of comet photon emission. We benchmark our calculations with x-ray emission data from JPL for 3 keV/amu collisions, and then with the high-resolution calorimeter data from LLNL for 10 eV/amu collisions. The CTMC calculations are then used to make an *ab initio* prediction of the x-ray emission for comet C/Linear 1999 S4 by use of the ion abundances published for the slow and fast solar winds. We show that the satellite measured spectra are consistent with their origin due to electron capture collisions between the slow solar wind and the comet's coma.

II. THEORETICAL METHOD

We have performed classical trajectory Monte Carlo (CTMC) calculations of the cross sections for single electron capture [4,5]. This procedure involves numerically solving Hamilton's equations for a mutually interacting three-body system. While hydrogenic ions are represented by means of Coulomb potentials, for partially stripped ions the active electron is considered to evolve under the potential model developed by Green *et al.* from Hartree-Fock calculations [19] and later on generalized by Garvey *et al.* [20]. The CTMC method directly includes the ionization channel and is not limited by a basis set size for the prediction of capture to very high-lying excited states.

A classical number n_c is obtained from the binding energy E_p of the electron relative to the projectile by

$$E_p = -\frac{Z_p^2}{2n_c^2}, \tag{5}$$

where Z_p is the charge of the projectile core. Then, n_c is related to the quantum number n of the final state by the condition

$$[(n-1)(n-1/2)n]^{1/3} \leqslant n_c < [(n+1)(n+1/2)n]^{1/3}. \tag{6}$$

From the normalized classical angular momentum $l_c=(n/n_c)(\mathbf{r}\times\mathbf{k})$, where $\mathbf{r}$ and $\mathbf{k}$ are the captured electron position and momentum relative to the projectile, we relate l_c to the orbital quantum number l of the final state by

$$l \leqslant l_c < l+1. \tag{7}$$

The m_l determination is satisfied by

$$\frac{2m_l-1}{2l+1} \leqslant \frac{l_z}{l_c} < \frac{2m_l+1}{2l+1}, \tag{8}$$

where l_z is the z-projection of the angular momentum obtained from the calculations [12]. The cross section to a definite (n,l,m) state is then given by

$$\sigma_{nlm} = \frac{N(n,l,m)\pi b_{\max}^2}{N_{tot}}, \tag{9}$$

where $N(n,l,m)$ is the number of events of electron capture to the nlm level and N_{tot} is the total number of trajectories integrated. The impact parameter $b_{\max}$ is the parameter beyond which the probability of electron capture is negligibly small.

In order to obtain emission cross sections $\sigma^{(em)}_{n,l,m\rightarrow n',l',m'}$, cascade contributions from higher $n''>n$ levels are added and the n,l,m_l populations are multiplied by hydrogenic branching ratios $b_{l\rightarrow l'}$ for the relevant transitions [21] and by their relative line strengths [12]. In this sense, we have assumed the hydrogenic branching ratios to be valid for the high-lying singlet states of the He-*like* ions.

III. EXPERIMENTAL DETAILS

Our measurements were carried out at the Lawrence Livermore EBIT-I electron ion trap, making use of the magnetic trapping mode of operation [22,23]. In this mode, the electron beam is turned off after production of highly charged ions and EBIT is operated like a Penning trap. In the absence of the electron beam, the ions are confined on the order of seconds in the 3-T magnetic field generated by superconducting Helmholz coils and the potential applied to the outer electrodes of the cylindrical trap. The trapping potential limits the energy of the ions, as ions with sufficient kinetic energy can overcome the potential barrier and leave the trap. The low-Z ions shown here were confined by a 100-V barrier. Based on earlier measurements, these conditions mean that the temperature of the ions was 10 ± 4 eV/amu.

Because the ions are generated *in situ*, transfer losses are avoided and as many as 10^7 ions are available for study. Electron capture was induced by ballistic injection of gases. The injector was operated either in a continuous mode [22]

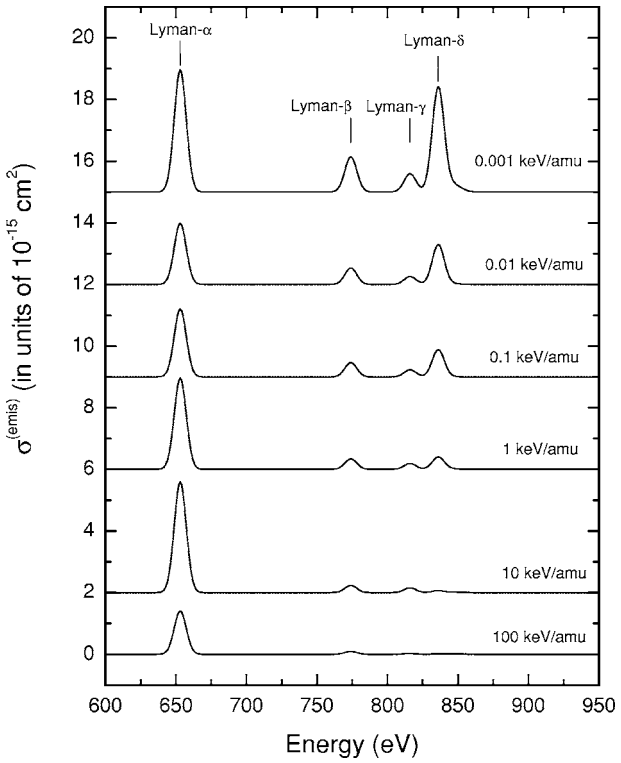

FIG. 1. CTMC emission cross sections after one electron capture by O^{8+} projectiles from a hydrogenic system. The collision energies are ranged from 1 eV/amu to 100 keV/amu. The binding energy for H_2O has been explicitly considered. The Lyman lines positions associated with the $np \rightarrow 1s$ transitions are explicitly shown. The results for 0.001, 0.01, 0.1, 1, and 10 keV/amu have been shifted for better visualization by 15, 12, 9, 6, and 2 (in units of 10^{-15} cm^2), respectively.

or in a pulsed mode [24]. X-ray spectra were recorded using a high resolution microcalorimeter.

We used the spare x-ray microcalorimeter spectrometer (XRS) from the ASTRO-E satellite mission. The XRS consists of a 6×6 pixel array with 32 active channels, forming a combined active area of 13 mm^2 that is operated at 59 mK [25]. The XRS was designed to view extended objects, such as supernova remnants, and has an energy resolution better than 10 eV. This resolution is an order-of-magnitude better than traditional Ge or SiLi detectors, and allows us to distinguish discrete lines associated with $np \rightarrow 1s$ Lyman x-ray transitions following electron capture collisions [26,27].

IV. ELECTRON CAPTURE AND LINE EMISSION CROSS SECTIONS

To put the energy dependence of the line emission cross sections into perspective, we present in Fig. 1 CTMC calculations for the O^{8+}+B system at energies from 1 eV/amu to 100 keV/amu, where the ionization energy of the target was chosen to represent that of the H_2O system. We note that the atomic hydrogen system has been studied with success by means of quantum mechanical theories (see, for example [28] and references therein). However, similar data for more involved systems is scarce. On the other hand, CTMC results have been presented during the years for collisions involving partially and fully stripped ions with multielectronic targets like Li, providing an accurate description of the measured emission lines [29,30]. The CTMC results neglect the detailed molecular states associated to the vibrationally excited levels of the target, instead it is reasonably assumed than an infinite number of energetic curve crossings are available for electron capture. We now describe the emission cross sections for an hydrogenic target. We use them as a benchmark to understand those corresponding to the molecular systems considered below, since the latter are the main concern of the present work.

Easily observed are the $2p \rightarrow 1s$, $3p \rightarrow 1s$, $4p \rightarrow 1s$, and $5p \rightarrow 1s$ Lyman transitions at approximately 653, 774, 816, and 836 eV, respectively. Here we have used a full width at half maximum (FWHM) resolution of 10 eV, which corresponds to that obtained using a microcalorimeter spectrometer. For all energies, if one inspects the n-level distributions of the O^{7+*} ion after electron capture, we find that the $5l$ levels dominate the overall total cross section. For energies lower than a few keV/amu the $5l$ contribution is over 80% of the total cross section. By 100 keV/amu ionization of the active electron dominates, not electron capture, and the n-level distribution broadens considerably with the $n=5$ level now only receiving 13% of the capture flux. Below 1 keV/amu, the $n=5$ state selective electron capture fraction changes relatively slowly. However, this is not the case for the l-sublevels within a given n-state. Because of the dipole selection rule $\Delta l = \pm 1$, it is readily apparent that there is a strong energy dependence of the population of the np sublevel, and this is central to our understanding of the x-ray line emission.

In Fig. 2 we display the l-distributions for the $n=5$ level of the $O^{8+}+H_2O$ systems shown in Fig. 1. As is implied by the x-ray line emission cross sections of Fig. 1, the np levels are preferentially populated via low energy collisions. One can understand this energy trend using some rough approximations. In freshman physics we learn that $\mathbf{l}=\mathbf{r}\times\mathbf{p}$. If we view the collision in the projectile frame of reference, the projectile sees the active electron advancing toward it (in atomic units) with an angular momentum of $\mathbf{l}=\mathbf{b}\times\mathbf{v}$, where b is the impact parameter and v is the collision speed, where the mass of the electron is set equal to $m_e=1$ a.u. In order to estimate an overall value of b, we use

$$Q = \frac{1}{2}\pi b^2 = q10^{-15}\ \text{cm}^2, \tag{10}$$

which leads to an impact parameter value of

$$b = (5a_0)q^{1/2}, \tag{11}$$

and a preference for orbital angular momentum values of

$$l = 5q^{1/2}v. \tag{12}$$

If we use O^{8+} as an example, from the last equation the np-level will be highly populated at a collision speed of 0.07 a.u., corresponding to about 100 eV/amu. Such is the general trend displayed in Fig. 2 and helps to illustrate the energy dependence of the l levels.

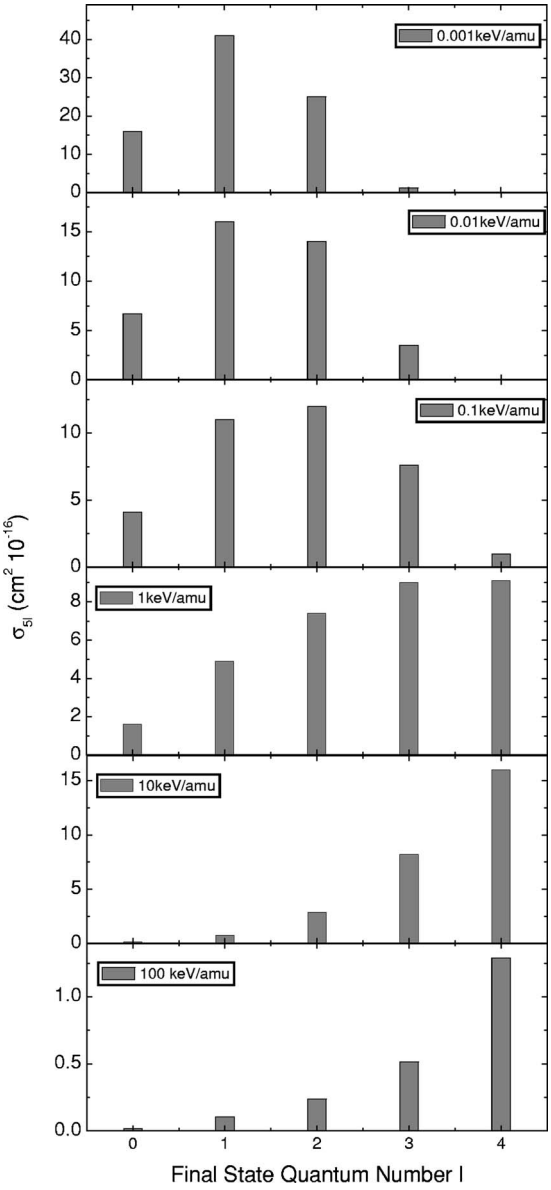

FIG. 2. CTMC electron capture cross sections into the $5l$ levels for O^{8+}-H_2O collisions with impact energies between 1 eV/amu and 100 keV/amu.

Although Eqs. (10)–(12) are not exact, and should be considered a rough approximation to the exact dynamics for these state-selective collisions, they approximately determine the preferred l levels to be populated at a certain impact energy.

For many measurements of x-ray spectra, it is usual to employ a Ge or a SiLi detector whose FWHM resolution is on the order of 100 to 250 eV. Thus, with these detectors one cannot directly test the energy dependence of the line emission cross sections presented in Fig. 1. It is possible, however, to employ a "hardness ratio" R that is defined as the line emission cross sections for the $np \rightarrow 1s$, $n>2$, divided by that for the Lyman-α $2p \rightarrow 1s$ value. In Fig. 3 we show the values obtained from the O^{8+} CTMC results of Fig. 1 along with the experimental value at 3 keV/amu obtained by Greenwood *et al.* [27] for O^{8+} on H_2O which has an

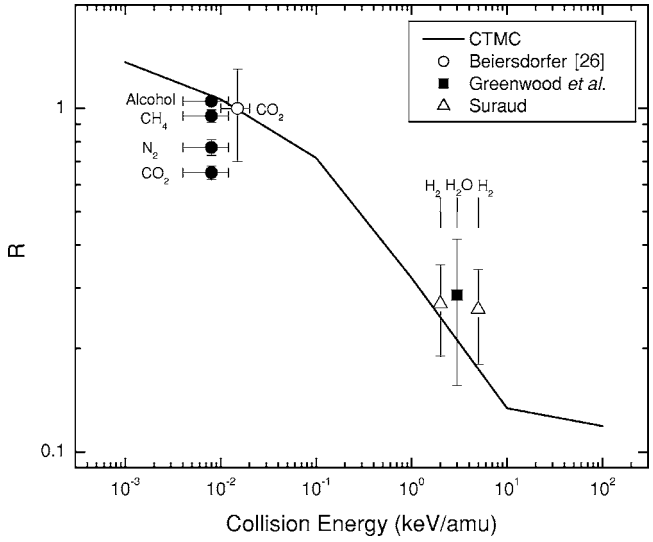

FIG. 3. Hardness ratio R as a function of the collision energy for O^{8+} projectiles. The experimental data of Biersdorfer at 15 eV/amu, Greenwood *et al.* [27] at 3 keV/amu, and Suraud at 2 and 5 keV/amu are included for comparison. The corresponding targets are explicitly shown.

ionization potential (12.6 eV) close to that of atomic hydrogen (13.6 eV). Displayed at 10 eV/amu is the hardness ratio measured in this work for O^{8+} colliding with CH_4 (IP=12.6 eV), CO_2 (13.8 eV), and N_2 (15.58 eV) targets. Qualitatively, there is reasonable agreement between theory and experiment, with our calculations tending to underestimate the magnitude of the population of the high-lying np states. Moreover, the rapid energy dependence of the ratio is nicely reproduced by the calculations. We have also included the hardness ratio values for H_2 (IP=15.43 eV) at 2 keV/amu and 5 keV/amu [31,32].

It can be seen that the experimental data is in very good agreement with the CTMC results at the collision energies considered. Furthermore, we can see that above about 10 keV/amu, the ratio approaches the statistical limit of $(2l+1)/n^2$, where $l=1$ for the np state and $n=5$ for the oxygen system. This leads to a hardness ratio of 0.12. Note that this value is not an absolute high energy limit since at very high collision energies the electron capture reaction populates a broad band of n levels whose maximum value shifts to low n values at collision speeds greater than about two times the orbital speed of the active electron that is being captured.

In Fig. 4 we compare our calculated line emission cross sections with those of Greenwood *et al.* [27,33]. Here we show the 3 keV/amu data for O^{8+} and Ne^{10+} on H_2O, and Ne^{10+} on He (IP=24.6 eV). Our cross sections have been convoluted with the experimentally reported energy resolution FWHM value of 102 eV and the photon Be window transmission of the Ge detector. For the three systems, it appears that a somewhat larger FWHM would have improved the agreement. However, it has been recently pointed out that double capture contributes to the low energy side of the Lyman-α peak and its inclusion could improve the agreement with the available data [17]. For the two Ne^{10+} systems,

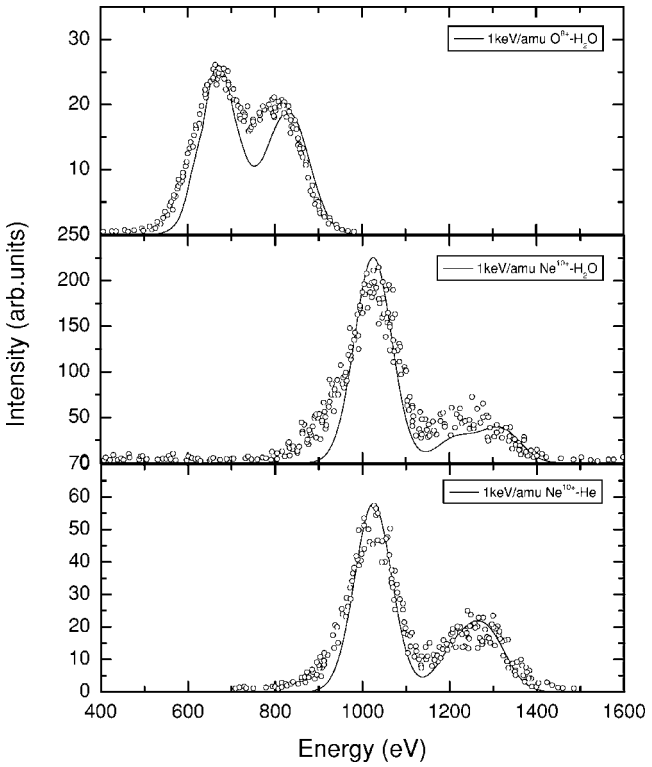

FIG. 4. Emission cross sections after single electron capture in 1 keV/amu collisions of O^{8+} and Ne^{10+} on H_2O and Ne^{10+} on He. The uncorrected experimental data of Greenwood *et al.* for the detector Be transmission window is represented by open circles and normalized to the theoretical results. The CTMC theoretical results have been degraded by means of 102 eV FWHM Gaussian functions.

the agreement is reasonable and illustrates the general dependence of the electron capture to populate lower n-levels for targets with a high ionization potential such as Ne, Eq. (4). The Greenwood *et al.* set of data has also been analyzed by Rigazio *et al.* using a LZ-based model. They found that minor corrections were needed in their capture probabilities to obtain good agreement with the data.

In Fig. 5 we compare the single charge exchange cross sections in H_2O, CH_4, and CO_2 measured by Greenwood *et al.* [33,34] for different ion charges with the present CTMC results. In the mentioned work, the experimental trends were considered indicative that the capture is not driven to a unique n level, but a range of states. This is in contrast with the classical overbarrier model predictions, which produce discontinuities due to the assumption that a single (charge-dependent) level is populated in the charge exchange. Although the absolute magnitudes are somewhat underestimated, the present CTMC results provide a good description of the experimental trends, mainly the slope with which the capture cross section increases as a function of the projectile ion charge.

In Fig. 6 we display a set of data from the EBIT for 10 eV/amu Ne^{9+} and Ne^{10+} on Ne (IP=21.6 eV). In both systems the data are taken using a Ge detector which has a FWHM energy resolution of 235 eV. For both cases we also present high resolution measurements obtained using the microcalorimeter that has an energy resolution of 10 eV. Our CTMC calculations have been convoluted by both of these resolutions. For Ne^{9+} the agreement with theory is reasonable. The He-*like* states produced after electron capture deemphasize the importance of the $np \rightarrow 1s$ $(n>2)$ line emission. We have used a statistical weight of 25% for the singlet states which can give rise to these Lyman transitions. Thus, their contributions to the spectra are almost negligible and barely observable on the figure in the 1070 to 1160 eV energy range. The triplets cannot contribute to the $np \rightarrow 1s$ transitions since their lifetimes are too long compared to those for transitions to lower triplet n-levels above the value of unity. Even though our hydrogenic branching ratios for the Lyman-β, γ, δ underestimate those for the He-like Ne [35], we have checked that the differences with the present emission cross sections are within the widths of the lines presented.

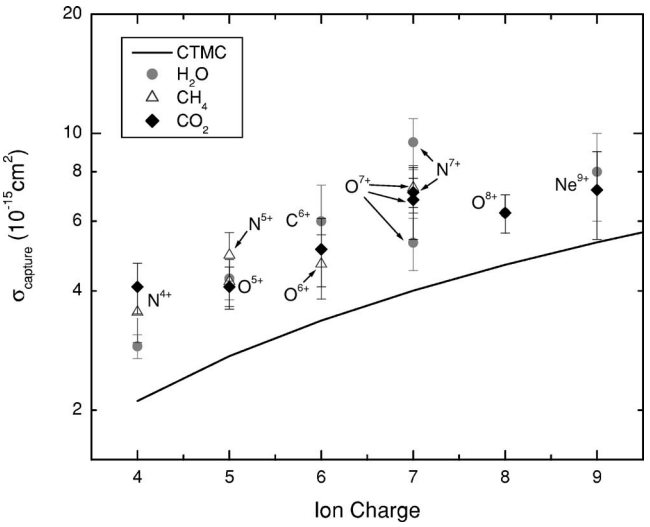

FIG. 5. Total single electron capture cross sections in 7 q keV collisions of O^{q+}, N^{q+} and Ne^{q+} on H_2O, CH_4, and CO_2 as a function of the initial projectile charge. The absolute experimental data corresponds to Greenwood *et al.* as given in Refs. [33,34].

The lower part of Fig. 6 displays the calculations and experiment for the Ne^{10+}+Ne system. For the Ge data, the calculations underestimate the $np \rightarrow 1s$ transitions by approximately 25%. When the microcalorimeter data is compared to theory, we can readily see the origin of the discrepancy. Theory greatly underestimates the $3 \rightarrow 1$ transition. This discrepancy we attribute to our neglect of double and multiple capture transitions followed by an Auger stabilization to a Ne^{9+*} ion that then radiatively cascades to the ground level. Previous studies have placed the double electron capture cross sections at approximately 25% of the single for this system [36,37].

However, one must be careful in that this fraction only represents the double capture states that are stable to decay. One must consider the fraction of single capture that arises from multiple capture events that are subsequently stabilized by intermediate Auger decay. For a multiple electron target such as Ar being collided by a 10+ ion projectile, single capture due to the multiple electron transfer can be 50–80 % of the value for single transfer [37]. For Ne we would expect a somewhat larger ratio.

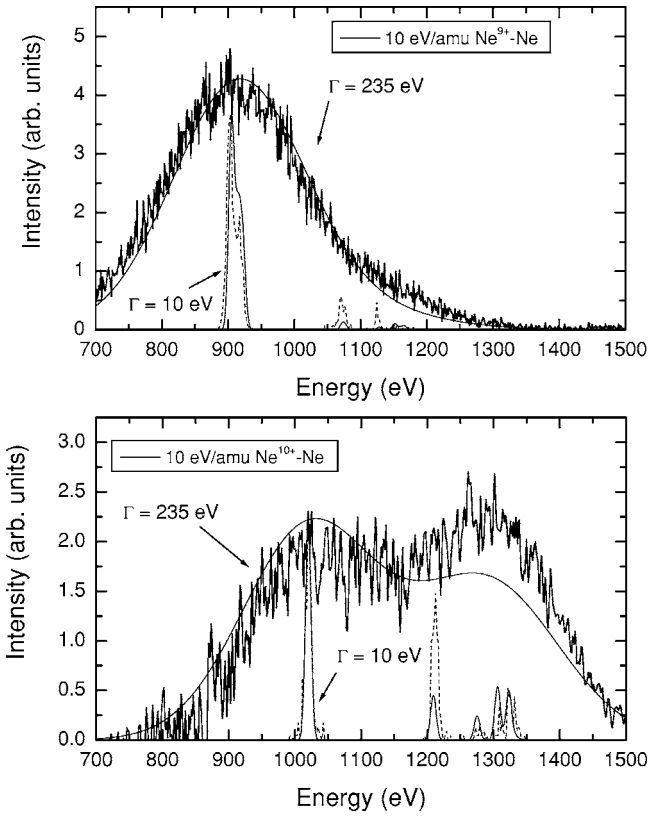

FIG. 6. Emission cross sections for 10 eV/amu Ne^{9+} and Ne^{10+} collisions with Ne. Experimental data of Beiersdorfer *et al.* [26] using a SiLi detector which has a FWHM energy resolution of 235 eV (solid-line) and a modern microcalorimeter that has an energy resolution of 10 eV (dashed line) are included. Theoretical results degraded to both resolutions are shown.

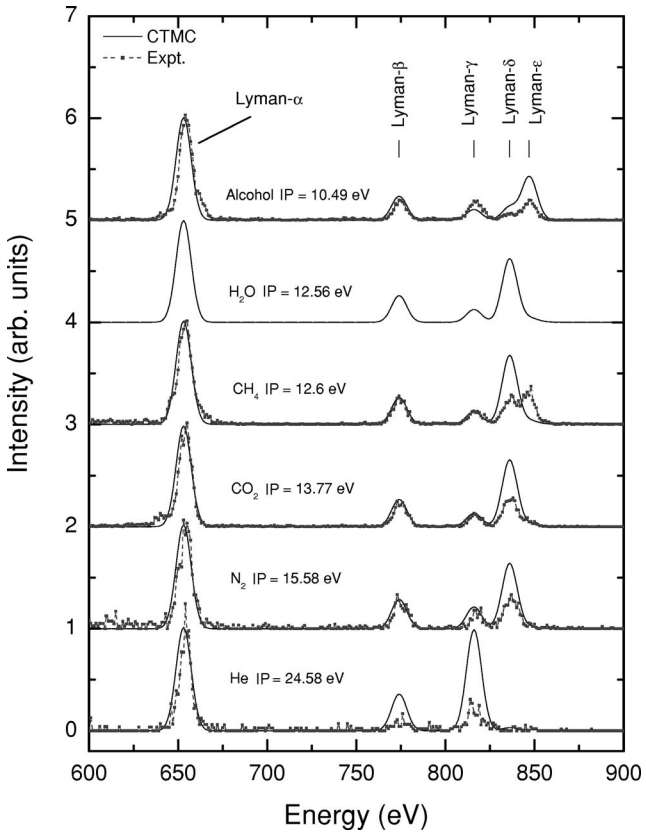

FIG. 7. Emission cross sections for 10 eV/amu collisions of O^{8+} with several atomic and molecular targets. Experimental data obtained with the 10 eV energy resolution microcalorimeter is included for comparison where available.

We can estimate the multiple transfer contribution to the Ne^{9+} emission from the spectra of Fig. 6. Double capture will mainly populate the $5l5l'$ states. For a low-Z ion such as Ne^{8+**}, the doubly excited states will primarily Auger decay. Since a density of states argument preferentially places the ejected electron in a low lying continuum level, the remaining electron will be found around $n' < n/\sqrt{2}$, or in this case, $n'=3$. From here, the one electron Ne^{9+*} ion will radiatively decay and enhance the $3p \rightarrow 1s$ x-ray emission. We find out that our one electron calculations underestimate the Lyman-β transition by a factor of three, providing a clear indication of multiple capture. However, we should note that the theoretical hardness ratio is very close to experiment. This is because multiple electron capture is not simply added to that for single capture. Multiple capture removes flux from the small impact parameter collisions. However, for the ions studied here, the calculated probability for single capture is already at the 100% level for these impact parameters. Thus, multiple capture events mainly rearrange the $np \rightarrow 1s$ x-ray emission to lower n levels, but do not change the overall magnitude of the hardness ratio.

The most demanding comparison of theory rests in measurements made for O^{8+} ions colliding with a series of atomic and molecular targets that have a large range of ionization potentials. Our purpose is to illustrate the dependence of the line emission cross sections on the target's ionization potential which is given qualitatively by Eq. (4). The collision temperature is 10 eV/amu. To represent the molecular targets, we have simply employed their ionization potential for the target in our hydrogenic CTMC calculations. The targets measured range from alcohol (IP=10.5 eV), to CH_4 (12.6 eV), CO_2 (13.8 eV), N_2 (15.6 eV), and He (24.6 eV). We also include our calculation for H_2O because of its relevance to astrophysical observations.

In Fig. 7 are the comparisons between theory and experiment. First, as a general observation, we observe the systematic shift of the dominant $np \rightarrow 1s$ Lyman x-ray transition from the $6p$ level for the low ionization potential alcohol, to the $5p$ level for the intermediate ionization potential molecules CH_4, CO_2, and N_2, while the high ionization potential He target system populates primarily the $4p$ level. Looking more closely, we observe the contribution from multiple electron capture for collisions with alcohol. In this system, the $n=6$ level is preferentially populated. Double capture to $6l6l'$ followed by Auger decay would lead to $O^{7+}(4l)$. Experimentally, there is a clear enhancement of the $4p$ state, implying the importance of multiple capture events. The other systems do not show a similar enhancement in the $3p$ or $4p$ levels.

V. APPLICATIONS TO COMET X-RAY EMISSION

Cometary x-ray emission was predicted in 1980 and the first attempt to detect it was with the Einstein Observatory [38]. Unfortunately, x-ray emission was not observed on that occasion. In this work, the prediction did not consider electron capture collisions but assumed the x-rays would result from plasma interactions between the comet and the solar wind. Furthermore, the emission was predicted to originate in the comet's tail.

It was not until 1996 that x-ray emission from a comet was successfully detected [39]. The Röntgen satellite (ROSAT) focused on the comet P/Hyakutake and observed x-ray emission of unexpected intensity from a region between the comet and the Sun out to a distance on the order of 10^6 km from the comet's nucleus.

By 2002, x-ray emission was observed and reported for fourteen comets [13]. Two models were proposed to explain the generation of cometary x-rays; (a) Bremsstrahlung and line emission from electron impact excitation collisions [40,41], and (b) electron capture between the heavy ions of the solar wind ions and the gas surrounding the comet [16]. In the former, the energetic free electrons created in the cometary plasma interact with the plasma ions, leading to Bremsstrahlung emission, and also excite the ions to produce line emission. However, a drawback is that x-ray emission has been observed out to great distances from the nucleus (10^5–10^6 km) where solar wind electrons are known to have energies of only 10 eV. Thus, they are incapable of exciting electronic levels that can lead to x-ray emission [13]. On the other hand, the latter mechanism considers electron capture by heavy ions in the solar wind with neutral cometary atoms or molecules. The excited ions produced after collisions, then emit x-rays when they cascade to their ground state [16].

Perhaps the clearest x-ray spectrum of a comet obtained to date was observed on July 14, 2000 and detected by the Chandra X-ray Observatory (CXO) [42]. The CXO measured the soft x-ray spectrum from the comet C/LINEAR 1999 S4, with high enough resolution for several lines to be evident. The comet disintegrated just a few days after the measurements. A laboratory simulation of charge-exchange-produced x-rays has proved to successfully reproduce the soft x-ray spectrum of the comet C/LINEAR 1999 S4 [43]. This indicated, from the experimental point of view, that an emission model based solely on charge exchange can account for the observed spectral structure.

In an attempt to model the x-ray emission from C/LINEAR 1999, we have employed the CTMC method to obtain absolute state-selective electron capture cross sections. These are coupled with hydrogenic branching and cascading simulations to predict the magnitudes of the x-ray emission lines. No adjustable parameters were used in our work. In Fig. 8(a) we present calculations for interactions of the fast solar wind (FSW) (~750 km/s) and slow solar wind (SSW) (~400 km/s) with H_2O by employing the ions abundance tabulated by Schwadron and Cravens [44]. Only ions with significant abundance having x-ray emission lines whose energies are above 300 eV are considered; C^{5+}, C^{6+}, N^{6+}, N^{7+}, O^{7+}, and O^{8+}. The triplet $2\,{}^3P \rightarrow 1\,{}^1S$ emission has been included for each of the He-like product ions. The theoretical results have been convoluted with the CXO ACIS-S detector's effective area (intensity response function) and degraded to its 100 eV FWHM energy resolution. The Chandra ACIS-S spectrum of July 14, 2000 is normalized to the SSW results. The measured spectrum is best reproduced by the SSW abundances even though the C^{6+} and O^{8+} contributions are somewhat overestimated by the tabulated abundances of Schwadron and Cravens. On the other hand, the FSW abundances lead to a very intense signal due to the C^{6+} ion with a low intensity from the O^{7+} ion. This is in contrast with the measured spectrum.

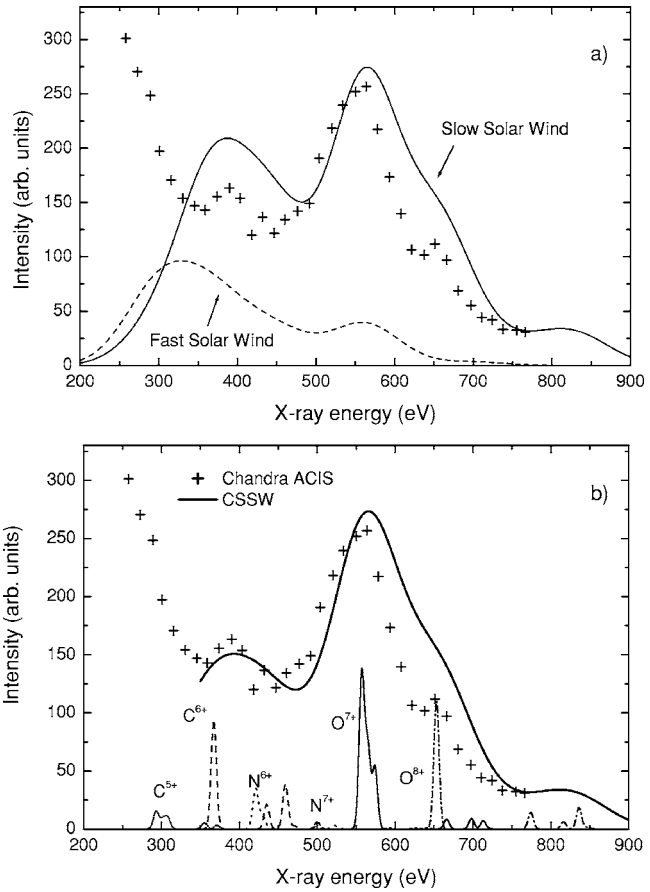

FIG. 8. CTMC x-ray emission spectrum for the comet C/LINEAR 1994 S4. (a) FSW and SSW spectra according to the ionic abundances of Schwadron and Cravens. The Chandra-ACIS measured spectrum is normalized to the SSW. (b) Corrected CTMC spectrum by modifying the SSW tabulated abundances of C^{6+} as shown in Table I.

It is important to state that the tabulated abundances of Schwadron and Cravens were obtained by averaging data obtained over a long period of time from Ulysses/SWICS (Solar Wind Ion Composition Spectrometer) and may not exactly reflect the charge state fractions for the different ions on the day that the CXO x-ray spectrum was measured. We note that the C^{5+} to C^{6+} ratio measured by the Advanced Composition Explorer ACE/SWICS-SWIMS (Solar Wind Ions Mass Spectrometer) on the day of the x-ray measurements, July 14, 2000 equals 1.03 [45].

We have incorporated the later ion ratio in what is termed corrected slow solar wind CSSW; the abundances are given

TABLE I. Ion abundance fractions employed in our calculations of x-ray emission from the C/LINEAR 1999 S4 comet. The notation is FSW (fast solar wind) and SSW (slow solar wind) where the ratios are taken from the work of Schwadron and Cravens [44]. The last column CSSW are the SSW abundances modified by the C^{5+} to C^{6+} ratio measured on 14 July 2000 by the ACE satellite.

	Abundances $[X^{q+}/O]$		
Ion species	FSW	SSW	CSSW
C^{5+}	0.440	0.210	0.210
C^{6+}	0.085	0.318	0.204
N^{6+}	0.011	0.058	0.058
N^{7+}	0.000	0.006	0.006
O^{7+}	0.030	0.200	0.200
O^{8+}	0.000	0.070	0.070

in Table I. On the bottom of Fig. 8 are displayed our *ab initio* x-ray line emission calculations with the updated CSSW values. The simulation of the data are quite good except that the abundance of the O^{8+} ion appears to be overestimated, yielding a more pronounced shoulder on the O^{7+} dominant line at about 650 eV than is present in the measurement. However, overall the agreement between the CTMC generated cross sections and the data are reasonable if one assumes the spectrum originated from interactions of the gas in the comet's coma and slow solar wind ions. We have also compared the CSSW abundances with those obtained by Beiersdorfer [43] from x-ray measurements following the charge exchange between the mentioned ion species and CO_2. We found good overall agreement with only the O^{8+} and C^{5+} abundances being slightly outside the experimental error bars.

VI. CONCLUSIONS

In this paper we have presented a theoretical description of state-selective electron capture collisions that lead to the emission of x-rays. The CTMC method has been employed to calculate the capture cross sections. The state specific nl-values are then used as input for a code that follows the branching and cascading of the excited levels until they reach the ground state. Both programs, in principle, are valid only for hydrogenic systems. We have varied the ionization potential of the target in order to simulate molecules with various ionization potentials, and have assumed the hydrogenic branching ratios are sufficiently accurate to predict the spectra for the high-lying singlet states of heliumlike ions.

Comparison with high resolution microcalorimeter data indicates the importance of multiple capture events followed by Auger decay in the line emission cross sections. However, since flux must be conserved and the calculated single capture probabilities are already at 100% for the impact parameters important to multiple capture, the calculated hardness ratios follow closely experimental values for both magnitude and energy dependence. The target-dependence of the hardness ratio values has been explicitly shown by considering different molecular targets with similar ionization potentials. The signature of multiple capture events is the enhancement of emission from the $n_p/\sqrt{2}$ level. This was clearly observed in the Ne^{10+}+Ne microcalorimeter data.

Our work is motivated by recent observations of x-rays from comets as they transit our solar system. We have concentrated on multiply charged ion species that are significant components of the solar wind and play an important role in the x-ray observations. Here, we have satisfactorily benchmarked our calculations to those of Greenwood *et al.* [27,33] who have measured line emission cross sections for systems and energies of direct importance to this study. We have been able to nicely reproduce Chandra satellite information obtained when it viewed C/LINEAR 1999 S4. This spectrum is particularly important since the solar wind composition and respective ion concentrations were being measured simultaneously by two other satellites. The measured ion concentrations were combined with our *ab initio* absolute line emission cross sections to compare to the observed satellite spectra.

Part of the study has been to illustrate how the x-ray patterns change with different targets, showing that line emission emphasizes higher n levels with low ionization potential targets than with large ionization potentials. Likewise, we show how the l values and the line emission cross sections change with collision energy. The latter study is important since it unifies the existing benchmark measurements that are made at 10 eV/amu and 3 keV/amu and are several orders-of-magnitude apart in energy. Both experimental techniques provide valuable tests of theory.

The microcalorimeter measurements displayed in this paper illustrate the resolution that will be available with the next generation satellite x-ray observatory. A prototype of the detector employed here will be used on a future ASTRO-E satellite mission. With a successful launch, the details of electron capture collisions between solar wind ions and the molecular targets in the comet's coma will help further our understanding of our solar system.

ACKNOWLEDGMENTS

This work was supported by the Office of Fusion Energy Sciences, DOE. We would like to thank Dr. R. Hoekstra for helpful discussions and a critical reading of the manuscript.

[1] W. Fritsch and C. D. Lin, Phys. Rep. **202**, 1 (1991).
[2] N. Shimakura, S. Suzuki, and M. Kimura, Phys. Rev. A **48**, 3652 (1993).
[3] A. Salop and R. E. Olson, Phys. Rev. A **13**, 1312 (1976).
[4] R. Abrines and I. C. Percival, Proc. Phys. Soc. London **88**, 873 (1966).
[5] R. E. Olson and A. Salop, Phys. Rev. A **16**, 531 (1977).
[6] J. A. Perez, R. E. Olson, and P. Beiersdorfer, J. Phys. B **34**, 3063 (2001).
[7] R. E. Olson, K. H. Berkner, W. G. Graham, R. V. Pyle, A. S. Schlachter, and J. W. Stearns, Phys. Rev. Lett. **41**, 163 (1978).
[8] R. A. Phaneuf, Phys. Rev. A **28**, 1310 (1983).
[9] R. E. Olson, Phys. Rev. A **24**, 1726 (1981).
[10] R. C. Isler and R. E. Olson, Phys. Rev. A **37**, 3399 (1988).
[11] H. Anderson, M. G. von Hellermann, R. Hoekstra, L. D. Horton, A. C. Howard, R. W. T. Konig, R. Martin, R. E. Olson, and H. P. Summers, Plasma Phys. Controlled Fusion **42**, 781 (2000).
[12] S. Schippers, P. Boduch, J. van Buchem, F. W. Bliek, R. Hoekstra, R. Morgenstern, and R. E. Olson, J. Phys. B **28**, 3271 (1995).
[13] T. E. Cravens, Science **296**, 1042 (2002).
[14] R. Wegmann, H. U. Schimdt, C. M. Lisse, K. Dennerl, and J. Englhauser, Planet. Space Sci. **46**, 603 (1998).
[15] R. M. Häberli, T. I. Gombosi, D. L. De Zeeuw, M. R. Combi, and K. G. Powell, Science **276**, 939 (1997).
[16] T. E. Cravens, Geophys. Res. Lett. **24**, 105 (1997).
[17] Matthew Rigazio, V. Kharchenko, and A. Dalgarno, Phys. Rev. A **66**, 064701 (2002).
[18] V. Kharchenko, Matt Rigazio, A. Dalgarno, and V. A. Krasnopolsky, Astrophys. J. **585**, L73 (2003).
[19] A. E. S. Green, D. L. Sellin, and A. S. Zachor, Phys. Rev. **184**, 1 (1969).
[20] R. H. Garvey, C. H. Jackman, and A. E. S. Green, Phys. Rev. A **12**, 1144 (1975).
[21] H. A. Bethe and E. E. Salpeter, *Quantum Mechanics of One- and Two-Electron Atoms* (Springer, Berlin, 1957).
[22] P. Beiersdorfer, L. Schweikhard, J. Crespo Lopez-Urrutia, and K. Widmann, Rev. Sci. Instrum. **67**, 3818 (1996).
[23] P. Beiersdorfer, R. E. Olson, G. V. Brown, H. Chen, C. L. Harris, P. A. Neill, L. Schweikhard, S. B. Utter, and K. Widmann, Phys. Rev. Lett. **85**, 5090 (2000).
[24] L. Schweikhard, P. Beiersdorfer, G. V. Brown, J. Crespo Lopez-Urrutia, S. B. Utter, and K. Widmann, Nucl. Instrum. Methods Phys. Res. B **142**, 245 (1998).
[25] R. L. Kelley, M. D. Audley, K. R. Boyce, S. R. Breon, R. Fujimoto, K. C. Gendreau, S. S. Holt, Y. Ishisaka, D. McCammon, T. Mihara, K. Mitsuda, S. H. Moseley, D. B. Mott, F. S. Scott, C. K. Stahle, and A. E. Szymkowiak, Proc. SPIE **3765**, 114 (1999).
[26] P. Beiersdorfer, C. M. Lisse, R. E. Olson, G. V. Brown, and H. Chen, Astrophys. J. Lett. **549**, L147 (2001).
[27] J. B. Greenwood, I. D. Williams, S. J. Smith, and A. Chutjian, Astrophys. J. Lett. **533**, L175 (2000).
[28] K. Richter and E. A. Solov'ev, Phys. Rev. A **48**, 432 (1993).
[29] R. Hoekstra, R. E. Olson, H. O. Folkerts, E. Wolfrum, J. Pascale, F. J. de Heer, R. Morgenstern, and H. Winter, J. Phys. B **26**, 2029 (1993).
[30] C. Laulhé, E. Jacquet, P. Boduch, M. Chantepie, N. Ghérardi, X. Husson, D. Lecler, and J. Pascale, J. Phys. B **30**, 2899 (1997).
[31] M. G. Suraud, R. Hoekstra, F. J. de Heer, J. J. Bonnet, and R. Morgenstern, **24**, 2543 (1991)
[32] R. Hoekstra, D. Ciric, F. J. de Heer, and R. Morgenstern, Phys. Scr., T **28**, 81 (1989).
[33] J. B. Greenwood, I. D. Williams, S. J. Smith, and A. Chutjian, Phys. Rev. A **63**, 062707 (2001).
[34] N. Djurić, R. Mawhorter, S. J. Smith, and A. Chutjian, in XXIV International Conference on the Physics of Electronic and Atomic Collisions, Rosario, Argentina, 2005, Tu094.
[35] I. M. Savukov, W. R. Johnson, and U. I. Safronova, At. Data Nucl. Data Tables **85**, 83 (2003).
[36] A. Müller and E. Salzborn, Phys. Lett. **62A**, 391 (1977).
[37] R. Ali, C. L. Cocke, M. L. A. Raphaelian, and M. Stockli, Phys. Rev. A **49**, 3586 (1994).
[38] H. S. Hudson, W. H. Ip, and D. A. Mendis, Planet. Space Sci. **29**, 1373 (1981).
[39] C. M. Lisse, K. Dennerl, J. Englhauser, M. Harden, F. E. Marshall, M. J. Mumma, R. Petre, J. P. Pye, M. J. Ricketts, J. Schmitt, J. Trümper, and R. G. West, Science **274**, 205 (1996).
[40] R. Bingham, J. M. Dawson, V. D. Shapiro, A. Mandis, and B. J. Kellett, Science **275**, 49 (1997).
[41] T. G. Northrop, C. M. Lisse, M. J. Mumma, and M. D. Desch, Icarus **127**, 246 (1997).
[42] C. M. Lisse, D. J. Christian, K. Dennerl, K. J. Meech, R. Petre, H. A. Weaver, and S. J. Wolk, Science **292**, 1343 (2001).
[43] P. Beiersdorfer, K. R. Boyce, G. V. Brown, H. Chen, S. M. Kahn, R. L. Kelley, M. May, R. E. Olson, F. S. Porter, C. K. Stahle, and W. A. Tillotson, Science **300**, 1558 (2003).
[44] N. A. Schwadron and T. E. Cravens, Astrophys. J. **544**, 558 (2000).
[45] http://www.srl.caltech.edu/ACE/ASC/level2/lvl2DATA_SWICS.html